

# On Interacting Particles in 1D and 2D

Joshua DM Hellier



Doctor of Philosophy  
The University of Edinburgh  
July 2018

# **Abstract**

Interface growth, and in particular the prediction of its rate, has long been a tough problem in statistical physics. In this thesis, I will outline my personal take on the matter, and will showcase a possible approach to it consisting of constructing a microscopic model on a lattice and using this to parametrise a large-scale model of the phenomenon. I will then discuss how to do this with multiple interacting particle species in play.

# **Declaration**

I declare that this thesis was composed by myself, that the work contained herein is my own except where explicitly stated otherwise in the text, and that this work has not been submitted for any other degree or professional qualification except as specified.

Parts of this work have been published in .

*(Joshua DM Hellier, July 2018)*

# **Acknowledgements**

Insert people you want to thank here.

# Contents

<b>Abstract</b>	i
<b>Declaration</b>	ii
<b>Acknowledgements</b>	iii
<b>Contents</b>	iv
<b>List of Figures</b>	vii
<b>List of Tables</b>	ix
<b>1 Preliminary Work, Background and Motivation</b>	1
1.1 The TiO <sub>2</sub> /Ti Interface System .....	1
1.2 Initial Attempts to Model the TiO <sub>2</sub> /Ti Interface System.....	1
1.2.1 The Difficulties of Nonequilibrium Statistical Mechanics ....	1
1.2.2 Dynamics of Ionic Crystals .....	1
1.2.3 Initial Work Done with MD .....	2
1.2.4 The Problems with MD.....	2
1.3 Simple Large-Scale Models of the Ti/O/Nb Interacting System .....	2
1.3.1 Proposed Linear System.....	2
1.3.2 Attempts to create a Suitable Nonlinear System .....	2

1.3.3	Parametrisation from a Microscopic Model .....	2
1.4	The Sticky Particle Model.....	3
1.4.1	Model Motivation .....	3
1.4.2	Model Definition .....	3
1.4.3	Model Properties .....	3
1.4.4	Relation to Existing Literature .....	3
1.4.5	Generalisation to Higher Dimensions.....	3
1.5	Implications of Initial Work for the PhD Direction.....	3
1.5.1	Why the Change of Direction?.....	3
1.5.2	Why Investigate Flow in the SPM?.....	3
<b>2</b>	<b>Analytical Results about the SPM</b>	5
2.1	Solving Problems in Nonequilibrium Statistical Mechanics.....	5
2.1.1	Equilibrium Statistical Mechanics.....	6
2.1.2	Nonequilibrium Statistical Mechanics .....	7
2.1.3	Where does the SPM stand? .....	7
2.2	Similarities between the SPM and Established Models in 1D.....	7
2.2.1	Relationship with the Ising Model .....	7
2.2.2	Correlation Functions .....	8
2.2.3	Equivalence with the Misanthrope Process .....	9
2.2.4	Differences Between SEP and the SPM.....	10
2.3	Using the Mean-Field Approximation on the SPM .....	10
2.3.1	Lattice MFT Derivation .....	11
2.3.2	Continuum Limit MFT Derivation.....	12

2.3.3	Negative Diffusion Coefficients.....	14
2.3.4	Continuum Limit MFT Solutions .....	17
2.3.5	Implications of Continuum MFT Breakdown.....	23
2.4	The SPM in Higher Dimensions.....	24
2.4.1	Symmetry + Locality + Detailed Balance = Unique 1-Parameter SPM .....	26
2.4.2	MFT of the $n$ -Dimensional SPM .....	30
<b>3</b>	<b>Numerical Results about the SPM</b>	34
3.1	Numerical Simulations of Continuous-Time Markov Processes .....	34
3.1.1	Known Methods.....	34
3.1.2	KMCLib.....	34
3.1.3	Running KMCLib on Eddie3.....	34
3.2	Calculation Results .....	35
3.2.1	1D .....	35
3.2.2	2D .....	35
<b>4</b>	<b>Conclusions</b>	36
<b>A</b>	<b>Code Listings</b>	37
A.1	1d Ising Correlation Functions .....	37
A.2	$n$ -Dimensional Continuum-Limit MFT .....	39
<b>Bibliography</b>		40

# List of Figures

(2.1) Plots of the equal-time particle density correlation function on a ring. . . . .	9
(2.2) Some plots of the variation of the MFT diffusion coefficient with density, for some selected $\lambda$ . . . . .	14
(2.3) A contour plot of the variation of the MFT diffusion coefficient with density and stickiness. . . . .	15
(2.4) The variation in the current at fixed $\lambda$ with respect to the boundary densities. . . . .	19
(2.5) The variation of flow rate with respect to $\lambda$ in the MFT, with fixed boundary densities. . . . .	20
(2.6) The dependence of the critial value of $\lambda$ required for backward diffusion on the boundary conditions. . . . .	21
(2.7) The variation of the system-wide average density with respect to $\lambda$ in the MFT, with fixed boundary densities. . . . .	22
(2.8) The possibe transitions which may occur in a symmetric local 2-dimensional hopping model. . . . .	25
(2.9) Figure demonstrating that a local system obeying detailed balance and symmetry cannot have interesting local configuration-dependent dynamics. . . . .	27
(2.10)Figure demonstrating that particle motion out of a hyperplane with $m$ adjacent particles away from an empty space moves with rate $\lambda^m$ . . . . .	29
(2.11)Figure demonstrating that particle motion out of a hyperplane with $m$ adjacent particles away from an empty space moves with rate $\lambda^m$ . . . . .	29
(2.12)2d SPM MFT current flow due to boundaries, for a selection of $\lambda$ . . . . .	33

(2.13) 2d SPM MFT current flow as a function of  $\lambda$ , with fixed boundaries. 33

# **List of Tables**

(2.1) The dependence of MFT current upon dimension in the SPM. . . 31

# **Chapter 1**

## **Preliminary Work, Background and Motivation**

Here we need to talk about the original intent of the project.

### **1.1 The $\text{TiO}_2/\text{Ti}$ Interface System**

A description of the initial problem upon which the project was based.

### **1.2 Initial Attempts to Model the $\text{TiO}_2/\text{Ti}$ Interface System**

#### **1.2.1 The Difficulties of Nonequilibrium Statistical Mechanics**

#### **1.2.2 Dynamics of Ionic Crystals**

Maybe mention Ewald sums, and the other issues with computations about materials.

### **1.2.3 Initial Work Done with MD**

I used some LAMMPS code to try to work with MD initially; melts and things.

### **1.2.4 The Problems with MD**

Need to explain why issues with using MD, and why I eventually decided it was not a useful technique for this problem; in particular, why MD is fundamentally flawed as a concept.

## **1.3 Simple Large-Scale Models of the Ti/O/Nb Interacting System**

I had a think about various methods I could use to tackle the system in question, and decided that the approach would be most likely to bear fruit would be a continuum-modelled bulk PDE system with appropriate boundary conditions between phases.

### **1.3.1 Proposed Linear System**

Simplest possible model, and why it failed.

### **1.3.2 Attempts to create a Suitable Nonlinear System**

Talk about why nonlinearity is necessary (as in, it just spits out the previous system again), and the difficulties of parametrising it.

### **1.3.3 Parametrisation from a Microscopic Model**

Talk about the Dresden conference and what I learned from it.

## **1.4 The Sticky Particle Model**

### **1.4.1 Model Motivation**

As in, why this is a good start in 1d.

### **1.4.2 Model Definition**

### **1.4.3 Model Properties**

Including Detailed Balance, symmetry, “locality”. Also mention that it is a Markov process.

### **1.4.4 Relation to Existing Literature**

### **1.4.5 Generalisation to Higher Dimensions**

Including a proof of detailed balance in arbitrary dimensions (on square lattice).

## **1.5 Implications of Initial Work for the PhD Direction**

### **1.5.1 Why the Change of Direction?**

Essentially, why trying to solve this particular problem is actually kind of silly, and why having a better theory of driven lattice flows would be more useful.

### **1.5.2 Why Investigate Flow in the SPM?**

Talk about how boundary-condition-induced flow on systems that would otherwise obey detailed balance hasn't really been done before. Bring it around to the

question: “Can we have interesting dynamics in a model whose bulk motion is symmetric and obeys detailed balance?”

# **Chapter 2**

## **Analytical Results about the SPM**

We now have a model, the SPM, which should represent the kind of behaviour we are interested in. In this chapter we will attempt to derive analytic results about how material flows in the model. Initially this was all done with the aim of producing an approximation to the behaviour in the hydrodynamic limit and thus informing us about the surface layer formation; however, as you will see the analytic predictions suggest that the flows could be quite interesting in their own right.

### **2.1 Solving Problems in Nonequilibrium Statistical Mechanics**

Models in nonequilibrium statistical mechanics which contain nontrivial interactions between components often produce interesting behaviour, hence the wide interest in these models. However, they usually prove to be difficult to “solve” in any concrete sense. In this section I will give a brief overview of solution methods in equilibrium statistical mechanics, why nonequilibrium statistical mechanics problems tend to be harder to solve, and how this affects the way we approach the SPM.

### 2.1.1 Equilibrium Statistical Mechanics

Equilibrium statistical mechanics is a bread and butter part of undergraduate physics, and there are a great many texts on the subject [4]. When we speak of “solving” an equilibrium statistical mechanics system, the gold standard is to be able to calculate relationships between the statistics of large-scale quantities as a function of the system constraints or their conjugates. This allows one to classify the system’s behaviour by making equations of state and identifying phase transitions (situations where at least some large-scale quantity statistics vary with respect to each other in a discontinuous manner). As you will see, the SPM itself is isomorphic to an equilibrium statistical mechanics model so long as we do not drive the system using boundary conditions (e.g. particle reservoirs with different concentrations).

#### Exact Solutions

A quantity of key interest in equilibrium statistical mechanics is the partition function, usually denoted by  $Z$ . Say we have a closed classical mechanical system maintained at constant temperature  $T$  by a heat bath, so only energy can enter and leave the system (the canonical ensemble). Let its state space be  $\Xi$ , and denote an individual microstate (specific configuration of the system) by  $\xi$ . Such a system must of course have a Hamiltonian  $H : \Xi \rightarrow \mathbb{R}$ . The canonical partition function for this system is defined to be

$$Z(\beta) = \int_{\Xi} d\xi e^{-\beta H(\xi)}, \quad (2.1)$$

with  $\beta T = 1$ , where the integrand on the right hand side is the familiar Boltzmann weighting. This quantity is extremely useful, because itself and its derivatives are directly related to the statistics of large-scale quantities. For example, the ensemble-averaged total energy  $\langle E \rangle$  satisfies

$$\langle E \rangle = -\frac{\partial \log Z}{\partial \beta} \quad (2.2)$$

If one is able to obtain an expression for the canonical partition function by analytic means, you can calculate essentially any statistical moment of any large-scale quantity you desire, and thus the system is “solved” in the sense we used above.

## **Approximations**

### **2.1.2 Nonequilibrium Statistical Mechanics**

#### **Exact Solutions**

Talk about stuff like ASEP. Remember to mention that only very specific models seem to be analytically solvable, in particular you can't have interactions and range in the current models.

#### **Approximations**

Approximations in noneq statmech

#### **Similarities and Differences Between Nonequilibrium and Equilibrium Statistical Mechanics**

### **2.1.3 Where does the SPM stand?**

Basically, why we can't analytically solve it, and so why performing mean-field approximation is a decent start.

## **2.2 Similarities between the SPM and Established Models in 1D**

In the previous section we have discussed the various approaches one might use when attempted to derive properties of a nonequilibrium statistical mechanical system. We will now try to put these ideas into practise on the SPM.

### **2.2.1 Relationship with the Ising Model**

If we implement the rules of the SPM on a periodic domain, we no longer have to deal with boundary conditions. In this special circumstance, we can find an

isomorphism between this model and the Ising model with fixed magnetisation. One does this by associating the Ising spins  $\sigma_i \in \{-1, 1\}$  with  $\rho_i \in \{0, 1\}$  via

$$\rho_i = \frac{1}{2} (1 + \sigma_i). \quad (2.3)$$

Recalling our proof that the SPM obeys detailed balance, we saw that the equilibrium probability of finding the SPM in a state containing  $N$  particle-particle adjacencies is proportional to  $\lambda^{-N}$ . If our Ising Hamiltonian is defined via

$$H = \frac{1}{2} \sum_{i=1}^L J \sigma_i \sigma_{i+1} \pmod{L}, \quad (2.4)$$

the probability of finding ourselves in a state with  $N$  paired spins is  $e^{-\beta NJ}$ , with  $\beta T = 1$ . The comparison with the SPM is now obvious; we set  $\log \lambda = \beta J$ . Thus  $\lambda$  in the SPM is simultaneously playing the role of the binding energy and temperature in the Ising model. !Try to compute average energy!

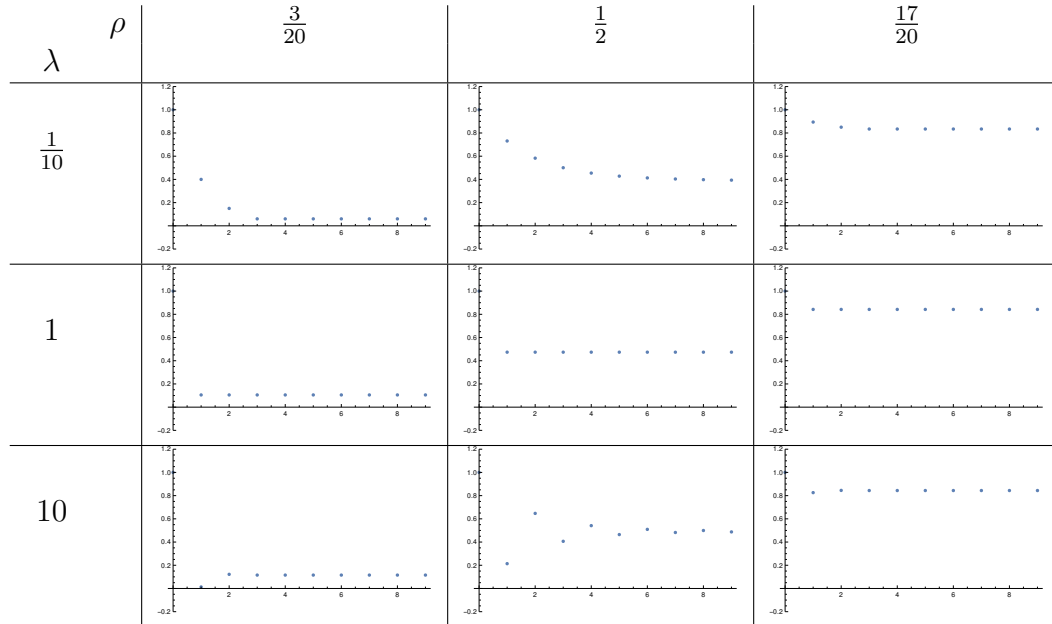
## 2.2.2 Correlation Functions

For relatively small systems, given a system size  $L$  and a number of particles  $N$ , we can analytically compute the pairwise correlation function  $C(l) = \langle \rho_i \rho_{i+l} \rangle$ , or “the probability that site  $i + l$  is occupied given that  $i$  is (the system is clearly homogeneous in  $i$ , so its value is irrelevant). A **Python** code which performs this calculations may be found in Sec. A.1

This is quite a nice result, as we can use simple recursion to perform a calculation which would otherwise be quite difficult to code. Unfortunately the time complexity of the calculation grows exponentially in  $N$  and  $L$ , so the largest  $L$  I can reasonably run for is 20. In the table below I have plotted the occupation probability of sites shifted from the origin (assuming the origin is occupied) for a selection of  $\lambda = e^{-b}$  and particle densities.

Clearly, as  $l$  becomes large, the correlation function tends to the density (note that the way we have define the correlation function it does not subtract this background probability; hence why many definitions do). Very small  $\lambda$ -values cause particles to tend to cluster together, whilst large  $\lambda$  values cause particles and vacancies to tend to alternate. In theory we could use the equivalence with the Ising model to compute correlation lengths as a function of  $\rho$  and  $\lambda$  by using the magnetic field in the original Ising model as a Lagrange

**Figure 2.1** Here are some particle-particle correlation functions for the SPM on a small closed ring, with the density chosen by choosing how many particles to insert at the start. The system in this case has 20 lattice sites. This was calculated using computer-assisted algebra and the various density and stickiness combinations should give an overall impression as to their structure.



multiplier in order to fix the total magnetisation (corresponding to particle number in the SPM). However, due to the fact that we cannot accurately compute correlation functions to any decent accuracy using our numerics (see Chap. ??), we concluded that it was not worth the time to perform the calculation as we would have nothing to compare it to.

### 2.2.3 Equivalence with the Misanthrope Process

Keeping the SPM on a ring, there is again a correspondence between it and the Misanthrope Process [1]. The Misanthrope Process is, like the SPM, defined by its rates. This time, however, there can be arbitrarily many particles on a single lattice site. We can choose to consider the symmetric version, in which particles hop in either direction. The defining feature of the process is that particles hop from sites with occupation  $m$  to adjacent sites with occupation  $n$  with some rate  $u(m, n)$ .

The equivalence between this and the SPM is made by identifying the **number** of particles on a site in the Misanthrope Process with the **length** of the gap between

two particles in the SPM. In this way, one can see that a particle moving, for example, one step right in the SPM corresponds to a particle moving from one stack to the adjacent one on the left in the Misanthrope Process. To complete the equivalence we set

$$u(m, n) = \begin{cases} \lambda, & n = 0 \\ 1, & \text{otherwise.} \end{cases}$$

Using the result from [1], that the probability weighting of a configuration  $\{m_i\}$  may be factorised as

$$P(\{m_i\}) \propto \prod_{i=1}^N f(m_i) \delta_{L+N, \sum_{j=1}^N m_j}, \quad (2.5)$$

where  $f(m)$  is a weighting dependant on the occupation of a site, we see that for the SPM  $f(m) = \lambda^{-m}$ . Thus, for finite  $\lambda$

$$\frac{f(m)}{f(m-1)} = \lambda^{-1} \quad (2.6)$$

which remains bounded as  $m \rightarrow \infty$ , therefore this model does not exhibit explosive condensation, again by using [1].

#### 2.2.4 Differences Between SEP and the SPM

### 2.3 Using the Mean-Field Approximation on the SPM

For the reasons discussed above, we cannot analytically solve the SPM on a nonperiodic bounded domain in the same way as SEP. It could be the case that a complete analytic solution method exists, but if it does, we do not know of it, so we will proceed on the assumption that the model is not analytically solvable. Therefore, it would be useful to at least possess approximate solutions, as this can help us by giving us something to test our numerics against, and point us in the direction of interesting behaviours which might occur. We will start by deriving the MFT on a lattice, and will then take the continuum limit (as the lattice

spacing tends to zero relative to our scale of interest), as that should predict the dominant behaviour on the macroscopic scale.

### 2.3.1 Lattice MFT Derivation

As usual, in an MFT approximation, we will be saying that the equal-time probability of the  $(i + 1)^{\text{th}}$  site being occupied is independent of the probability that the  $i^{\text{th}}$  site is occupied. More formally, let us denote the mean occupation of the  $i^{\text{th}}$  site at time  $t$  by  $\rho_i(t)$ . When we invoke the mean-field approximation, we say that the mean occupations of sites at equal times are independent; thus, the probability that site  $j \neq i$  occupied given that site  $i$  is occupied is  $\rho_j(t)$ . We can use this to calculate the rate at which  $\rho_i(t)$  increases and decreases, and so obtain a system of coupled ODEs for  $\rho_i(t)$ .

Let us first consider the situation where the  $i^{\text{th}}$  site is unoccupied. The probability of this being the case is  $(1 - \rho_i(t))$ . A particle could move from site  $(i - 1)$  or site  $(i + 1)$ , but only if those sites are currently occupied. Assuming that site  $(i - 1)$  is occupied (occurring with probability  $\rho_{i-1}$  in MFT), the rate at which it would jump to site  $i$  would depend on the occupation of site  $(i - 2)$ , as it would be 1 if it was unoccupied and  $\lambda$  if it was occupied. Phrasing this in MFT terms, and suppressing  $t$ -dependence for brevity, the rate at which  $\rho_i(t)$  is increased by particles coming from the left is

$$\tau_0^{-1} (1 - \rho_i) \rho_{i-1} [(1 - \rho_{i-2}) \cdot 1 + \rho_{i-2} \cdot \lambda]. \quad (2.7)$$

By symmetry, the income of particles from the right is

$$\tau_0^{-1} (1 - \rho_i) \rho_{i+1} [(1 - \rho_{i+2}) \cdot 1 + \rho_{i+2} \cdot \lambda]. \quad (2.8)$$

Using similar logic, but shifting things around slightly, the rate at which particles leave site  $i$  to go to site  $i + 1$  is

$$\tau_0^{-1} (1 - \rho_{i+1}) \rho_i [(1 - \rho_{i-1}) \cdot 1 + \rho_{i-1} \cdot \lambda], \quad (2.9)$$

and similarly

$$\tau_0^{-1} (1 - \rho_{i-1}) \rho_i [(1 - \rho_{i+1}) \cdot 1 + \rho_{i+1} \cdot \lambda] \quad (2.10)$$

is the rate at which particles leave  $i$  to go to  $i - 1$ .

At this point it becomes fairly clear why we introduced the quantity  $\zeta = 1 - \lambda$ , as it neatens things up in general. The total rate at which particles enter site  $i$  is

$$\tau_0^{-1} (1 - \rho_i) [(1 - \zeta \rho_{i-2}) \rho_{i-1} + (1 - \zeta \rho_{i+2}) \rho_{i+1}] \quad (2.11)$$

whilst they leave at rate

$$\tau_0^{-1} \rho_i [(1 - \zeta \rho_{i+1}) (1 - \rho_{i-1}) + (1 - \zeta \rho_{i-1}) (1 - \rho_{i+1})] \quad (2.12)$$

Combining the rates of arriving and leaving, we obtain our main result:

$$\begin{aligned} \tau_0 \frac{\partial \rho_i}{\partial t} &= (1 - \rho_i) [(1 - \zeta \rho_{i-2}) \rho_{i-1} + (1 - \zeta \rho_{i+2}) \rho_{i+1}] \\ &\quad - \rho_i [2\zeta \rho_{i-1} \rho_{i+1} - (3 - \zeta) (\rho_{i-1} + \rho_{i+1}) + 2]. \end{aligned} \quad (2.13)$$

This is a nice result, and in theory we could stop right here and we could make a computational scheme for solving this as a sequence. However, there are a few issues. For one thing,  $\rho_i(t)$  isn't the mean of a quantity whose variance is being suppressed by the law of large numbers, as is desired when using the MFT approximation. Thus, it is merely a rough sketch of what might happen, as variances and correlations between sites aren't suppressed. On the other hand, it simply relates the occupations of nearby sites, whereas we would find a description of the bulk flow to be much more useful. Therefore, we may as well take the continuum limit to see how flow depends on concentration gradient and local density.

### 2.3.2 Continuum Limit MFT Derivation

To take the continuum limit, let's promote  $\rho_i(t)$  to  $\rho(x, t)$  so that

$$\rho_{i+m}(t) \rightarrow \rho(x + am, t). \quad (2.14)$$

Now we can Taylor expand for  $\rho_{i+m}(t)$ , as

$$\rho(x + am, t) = \rho(x, t) + ma \frac{\partial \rho(x, t)}{\partial x} + \frac{1}{2} m^2 a^2 \frac{\partial^2 \rho(x, t)}{\partial x^2} + \mathcal{O}(a^3). \quad (2.15)$$

Preferably with the aid of a computational algebra package (in my case **Wolfram Mathematica**), one may directly substitute Taylor expansions for the required  $\rho_j$  into Eq. 2.13, continuing to truncate at  $\mathcal{O}(a^3)$ . Doing so, and collecting terms,

we find that

$$\tau_0 \frac{\partial \rho}{\partial t} = a^2 \left[ 1 - \zeta \rho (4 - 3\rho) \frac{\partial^2 \rho}{\partial x^2} \right] 2a^2 \zeta (3\rho - 2) \left( \frac{\partial \rho}{\partial x} \right)^2 + \mathcal{O}(a^4), \quad (2.16)$$

which may be factorised into the more convenient form

$$\frac{\partial \rho}{\partial t} = \frac{a^2}{\tau_0} \frac{\partial}{\partial x} \left\{ [1 - \zeta \rho (4 - 3\rho)] \frac{\partial \rho}{\partial x} \right\}, \quad (2.17)$$

which is a continuity equation

$$\frac{\partial \rho}{\partial t} = \frac{\partial J}{\partial x} \quad (2.18)$$

with current

$$J = -\frac{a^2}{\tau_0} [1 - \zeta \rho (4 - 3\rho)] \frac{\partial \rho}{\partial x}. \quad (2.19)$$

Considering Fick's Law

$$J = -D \frac{\partial \rho}{\partial x}, \quad (2.20)$$

we see that our diffusion coefficient is

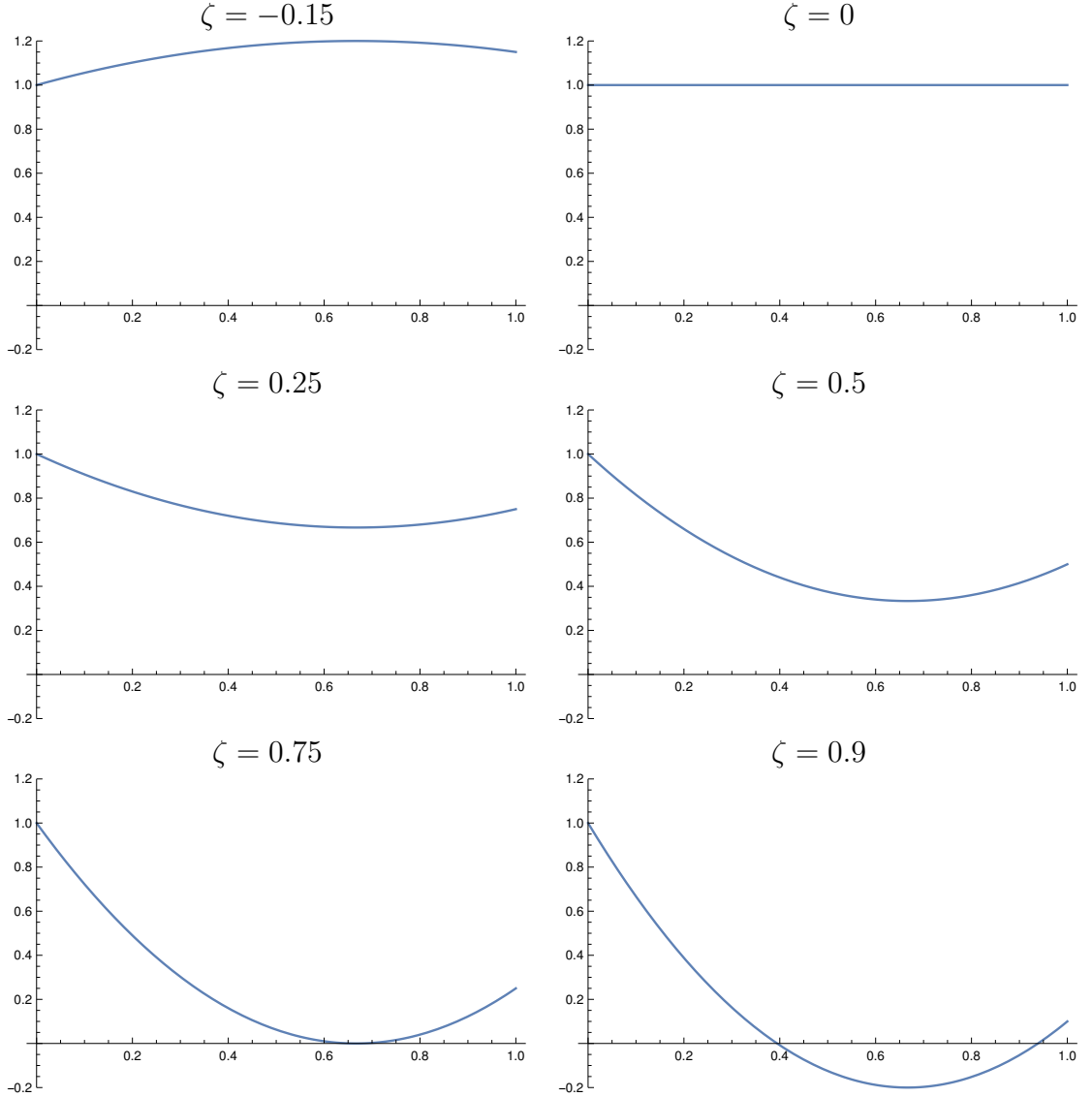
$$D = \frac{a^2}{\tau_0} [1 - \zeta \rho (4 - 3\rho)]. \quad (2.21)$$

Setting  $\zeta \rightarrow 0$  (i.e.  $\lambda = 1$ ), we see that  $D \rightarrow \frac{a^2}{\tau_0}$ , which is consistent with what we would expect for the Symmetric Exclusion Process.

Clearly, the diffusion coefficient varies quadratically with  $\rho$ . This is easiest to see via a few graphs, as shown in Fig. 2.2. Note that  $D \rightarrow \frac{a^2}{\tau_0}$  as  $\rho \rightarrow 0$  and  $D \rightarrow \frac{a^2}{\tau_0} \lambda$  as  $\rho \rightarrow 1$ , so for  $\zeta < 0$  ( $\lambda > 1$ )  $D$  is guaranteed to be positive for  $\rho \in [0, 1]$  as the diffusion coefficient is an inverted parabola so far as its variation in  $\rho$  is concerned.

Note that  $D$  has a symmetry in  $\rho$  around  $\rho = \frac{2}{3}$ , in the sense that  $D$  is unchanged under  $\rho \mapsto \frac{4}{3} - \rho$ . Why this symmetry is present in the MFT is a little unclear ( $\rho \mapsto 1 - \rho$  would be a much more obvious choice), however as you will see in the numerical simulations it does seem to be quite relevant, particularly in the high- $\lambda$  limit.

**Figure 2.2** Plots of the variation of  $\frac{\tau_0 D}{a^2}$  (y-axis) with respect to  $\rho$  (x-axis), evaluated with various values of  $\zeta$  (above plots).



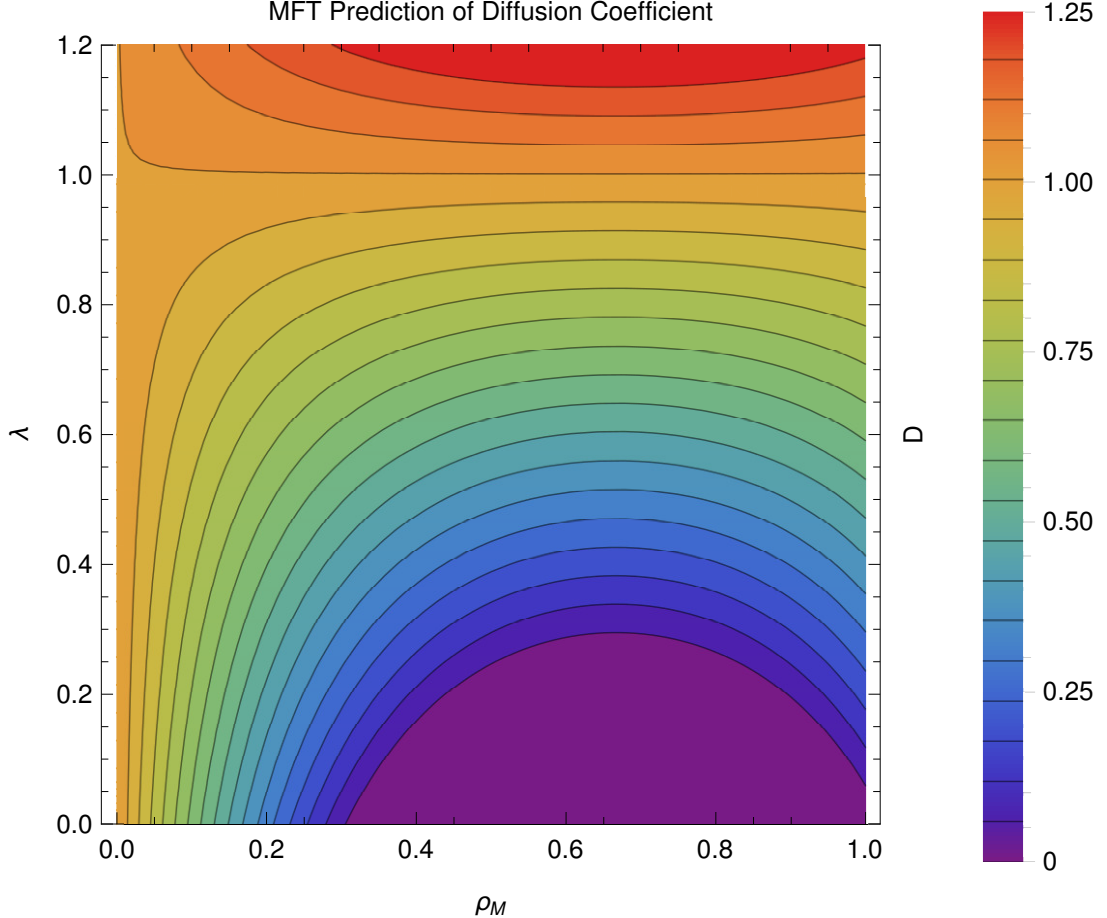
### 2.3.3 Negative Diffusion Coefficients

A quick inspection of the dependence of the diffusion coefficient  $D$  upon  $\zeta$  reveals that it is possible for strange things to happen in this MFT. For a given value of  $\zeta$ ,  $D$  is quadratic in  $\rho$ ; a natural question to ask is whether  $D$  is always positive, and if not, what the physical implications of this would be.

An easy way to do this is by analysing the roots of  $D$ . Writing it as a standard quadratic,

$$D = \frac{a^2}{\tau_0} [3\zeta\rho^2 - 4\zeta\rho + 1] \quad (2.22)$$

**Figure 2.3** A contour plot of the variation of  $\frac{\tau_0 D}{a^2}$  as a function of  $\rho$  and  $\lambda$ . The region with negative diffusion (which is really critically slow or zero diffusion due to our stability argument in 2.3.3) has been highlighted in purple. Note how as we descend in  $\lambda$  with  $\lambda < \frac{1}{4}$ , it grows from a single point at  $\rho = \frac{2}{3}$  to fill most physically realistic density values.



which has discriminant  $4\zeta \frac{a^4}{\tau_0^2} [4\zeta - 3]$ . For a real quadratic, the discriminant changes sign when the solutions switch between being real and complex, which in our case is the difference between having real solutions and not having real solutions. Assuming that  $\zeta > 0$  (as we know  $D$  is positive for  $\rho \in [0, 1]$  for  $\zeta < 0$ ), this change occurs when  $\zeta = \frac{3}{4}$  corresponding to  $\lambda = \frac{1}{4}$ , so there are no real solutions for  $\zeta < \frac{3}{4}$  and  $\lambda > \frac{1}{4}$ , and therefore  $D$  is guaranteed to be positive in these regions. Positive- $D$  is the normal situation in physics, and a solution to the MFT PDE Eq.2.17 which contains only positive- $D$  regions is at least self-consistent (although of course is only as good an approximation to the SPM as the continuum MFT assumptions allow).

When  $\zeta > \frac{3}{4}$ ,  $D$  is negative so long as

$$\frac{2}{3} - \frac{\sqrt{\zeta(4\zeta - 3)}}{3\zeta} < \rho < \frac{2}{3} + \frac{\sqrt{\zeta(4\zeta - 3)}}{3\zeta}; \quad (2.23)$$

this is like a gap opening up in  $\rho$  when  $\zeta > \frac{3}{4}$ . At its maximal extent (when  $\zeta = 1$ ), negative diffusion occurs for

$$\frac{1}{3} < \rho < 1, \quad (2.24)$$

so there is still a region where  $\rho$  is sufficiently low that negative diffusion does not occur.

In terms of what a negative diffusion coefficient actually means, consider a constant solution  $\rho(x, t) = \rho_0$ . Insertion Eq. 2.17 quickly confirms that this is indeed a solution. Now consider adding a small perturbation  $\delta\rho(x, t)$  to  $\rho_0$ . The equation for the time evolution of  $\delta\rho$  then reads

$$\frac{\partial\delta\rho}{\partial t} = \frac{a^2}{\tau_0} [1 - \zeta\rho_0 (4 - 3\rho_0)] \frac{\partial^2\delta\rho}{\partial x^2}. \quad (2.25)$$

This becomes a little clearer if one takes a Fourier transform with respect to  $x$ , so that  $\hat{\delta\rho}(k, t) = \mathcal{F}(\delta\rho(x, t))$ ; then, the equation of motion for  $\hat{\delta\rho}$  is

$$\frac{\partial\hat{\delta\rho}}{\partial t} = -k^2 \frac{a^2}{\tau_0} [1 - \zeta\rho_0 (4 - 3\rho_0)] \hat{\delta\rho}. \quad (2.26)$$

This shows us that so long as  $\zeta < \frac{3}{4}$ , small perturbations to the density are suppressed by exponential decay in time with increasing ferocity as their wavenumber increases for all wavenumbers, and so the solution is stable; the same applies if  $\zeta > \frac{3}{4}$  so long as we do not stray into situations where

$$\frac{2}{3} - \frac{\sqrt{\zeta(4\zeta - 3)}}{3\zeta} = \rho_- < \rho_0 < \rho_+ = \frac{2}{3} + \frac{\sqrt{\zeta(4\zeta - 3)}}{3\zeta}. \quad (2.27)$$

If we do find ourselves in this regime, small perturbations grow exponentially with time in a situation akin to ripening [find some decent references when possible], which, given that the particles are undergoing conserved flow, suggests that we will have a separation into regions with lower and higher densities. Of course, the positive feedback driving this separation stops if the density grows higher or lower than  $\rho_{\pm}$ , where we reenter the stable regime. This does suggest that in the MFT a system containing a negative- $D$  region would have a tendency to

self-organise itself into alternating domains, with at least the boundaries of these domains having densities of  $\rho_-$  or  $\rho_+$ . This is very important: whilst it is no coincidence that these critical values of the density are those densities where our diffusion coefficient is zero, this does suggest that **a solution to the continuum MFT in the  $\lambda < \frac{1}{4}$  regime which contains values for  $\rho$  in the critical gap  $[\rho_-, \rho_+]$  should admit no current.** The search for this predicted effect is in fact the main driving force behind this entire PhD project.

### 2.3.4 Continuum Limit MFT Solutions

The continuum-limit MFT has given us a partial differential equation for  $\rho(x, t)$ ; therefore, we should try to find some solutions to it, as these may give us clues as to what types of behaviour the SPM might exhibit.

#### Steady Flow Across a Bounded Domain

It's pretty obvious that  $\rho = \rho_0 = \text{const.}$  is a solution to the MFT PDE, and it takes only a little thought to notice that this is in fact the only spatially homogeneous solution available. If we instead look for a solution which lacks time dependence (i.e.  $\rho(x, t) = \rho(x)$ ), the PDE reduces to the ODE

$$-\frac{a^2}{\tau_0} \frac{d}{dx} \left( [1 - \zeta\rho(4 - 3\rho)] \frac{d\rho}{dx} \right) = 0. \quad (2.28)$$

Integrating both sides with respect to  $x$ , and using the fundamental theorem of calculus, we find that

$$-\frac{a^2}{\tau_0} [1 - \zeta\rho(4 - 3\rho)] \frac{d\rho}{dx} = J_0, \quad (2.29)$$

with  $J_0$  an arbitrary constant, which has been labelled as such in hindsight because it represents the constant current flowing through the system in a steady

state. Doing so again, we find that we can invoke the chain rule via

$$J_0(x - x_0) = -\frac{a^2}{\tau_0} \int dx \frac{d\rho}{dx} [1 - \zeta\rho(4 - 3\rho)] \quad (2.30)$$

$$= -\frac{a^2}{\tau_0} \int d\rho [1 - \zeta\rho(4 - 3\rho)] \quad (2.31)$$

$$= -\frac{a^2}{\tau_0} \rho [1 + \zeta\rho(\rho - 2)] \quad (2.32)$$

Thus with a little rearrangement we have  $x$  as a function of  $\rho$ , with  $\rho$  a cubic in  $x$ . We can in principle invert this to obtain  $\rho(x)$ , but let us first consider the appropriate boundary conditions to use.

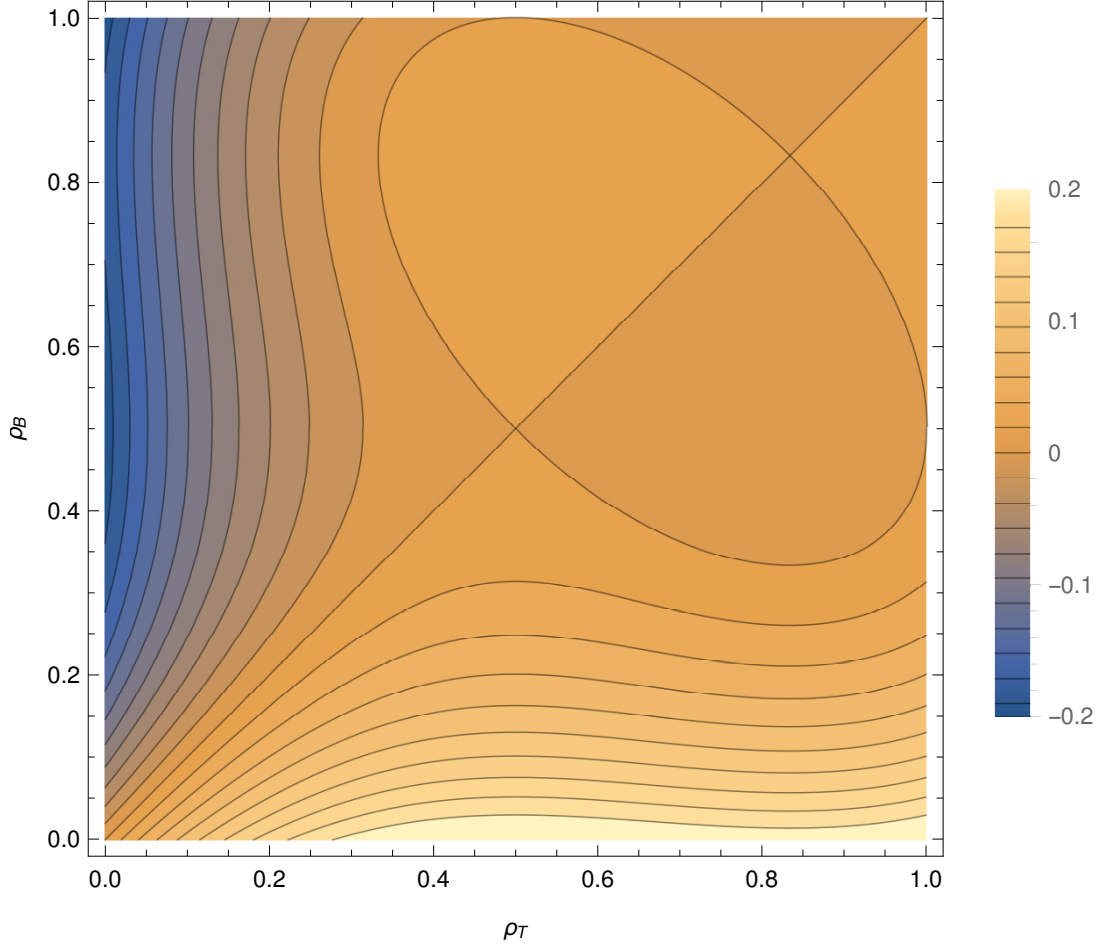
Let us consider solving problems on a bounded domain; we choose to do this as opposed to an infinite one, as one can see that for our cubic  $\|x\| \rightarrow \pm\infty \implies \|\rho\| \rightarrow \pm\infty$  for nontrivial  $J$ . Therefore let us consider solutions on the domain  $[0, L]$  for  $L > 0$ . With a second order ODE of this kind, we must supply two boundary conditions, which may be Dirichlet, Neumann or some mixture of the two, and must contain at least one piece of Dirichlet information. However, our ODE does not make any special reference to  $\rho$  values of 0 or 1, and therefore if we do not fix  $\rho$  at both boundaries it is highly likely that the solution will contain unphysical values for  $\rho$ . Therefore, let us apply Dirichlet conditions at both boundaries, so that  $\rho(0) = \rho_0$  and  $\rho(L) = \rho_L$ . Inserting this information into Eq. 2.30 we can fix the constants  $x_0$  and  $J_0$ ; in particular we find that

$$J_0 = \frac{a^2}{L\tau_0} [\rho_0 - \rho_L + \zeta (\rho_0 [\rho_0^2 - 2] - \rho_L [\rho_L^2 - 2])], \quad (2.33)$$

which can be reinserted to yield the desired  $x_0$ . An illustrative plot of  $J_0(\rho_B, \rho_T)$  is shown in Fig. 2.4.

This solution in particular is extremely useful, as we can use it to predict the flow which should occur (MFT being correct) if we set up a numerical simulation of the SPM with a length of, say,  $L$  lattice points. In particular, if we vary  $\lambda$  whilst keeping the boundaries constant, the measured current should vary linearly, as depicted in Fig. 2.5. Thus, if we were to run simulations with, say,  $(\rho_0, \rho_L) = (0.6, 0.4)$ , we should see the transition to a backwards or critically slow flow occur. We can use Eq. 2.33 to find the critical value for  $\lambda$ ,  $\lambda_c$ , at which the transition to negative diffusion should occur for given boundary conditions. To do this, we

**Figure 2.4** A contour plot of the variation of the constant current  $J_0(\rho_B, \rho_T)$  in a bounded domain with boundary densities  $\rho_0$  and  $\rho_L$  at  $x = 0$  and  $L$  with  $\lambda = 0.2$ . Notice how the magnitude of  $J_0$  generally grows as the difference between  $\rho_0$  and  $\rho_L$  increases, and how there is a region of boundary condition space in which the current takes the opposite sign one would expect.



simply set  $J_0 = 0$  and solve for  $\lambda$ , and find that

$$\lambda_c = 1 - \frac{1}{2(\rho_0 + \rho_L) - (\rho_0 + \rho_L)^2 + \rho_0 \rho_L}. \quad (2.34)$$

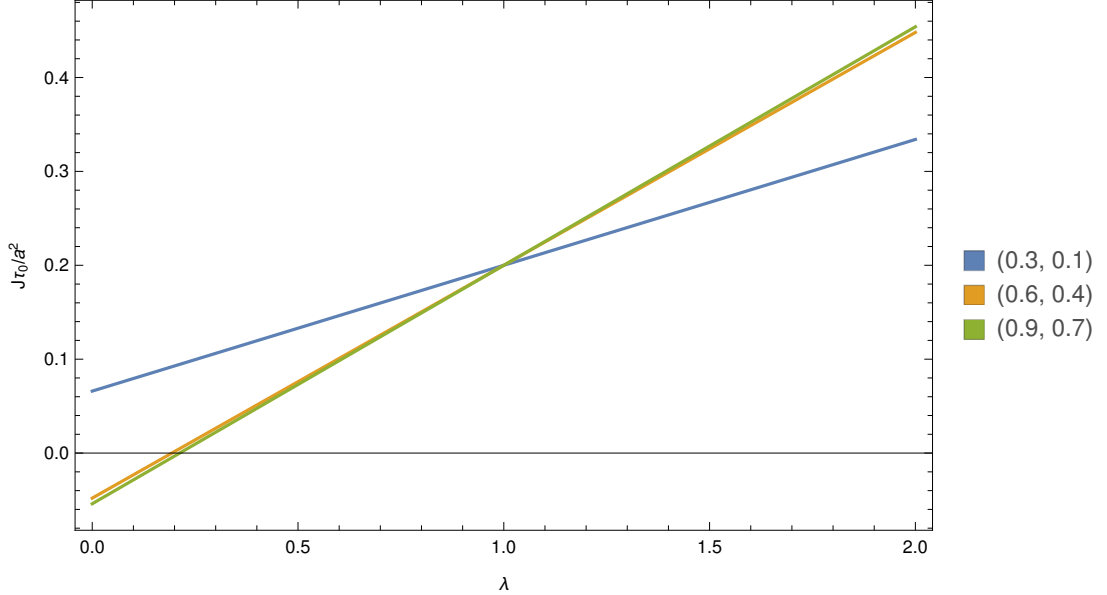
This is shown in Fig 2.6.

We can also obtain a prediction of the system-wide average density

$$\bar{\rho} = \frac{1}{L} \int_0^L dx \rho(x), \quad (2.35)$$

so long as we can invert  $x(\rho)$  to find  $\rho(x)$  uniquely. The easiest way to do this is

**Figure 2.5** A plot of the MFT prediction of the dedimensionalised flow rate with varying  $\lambda$  for boundaries  $(\rho_0, \rho_L) = \{(0.3, 0.1), (0.6, 0.4), (0.9, 0.7)\}$ . Notice how the dependence of  $J$  on  $\lambda$  is actually very similar for the high and medium boundary-density-average situations, but is quite different for the low density case. Note that the MFT clearly predicts that the flow should start running backwards when  $\lambda$  becomes sufficiently low, which means that we should be able to see backwards or critically-slow flow in our numerics if we hold the boundaries constant whilst varying  $\lambda$ .



using the main result in [3], yielding

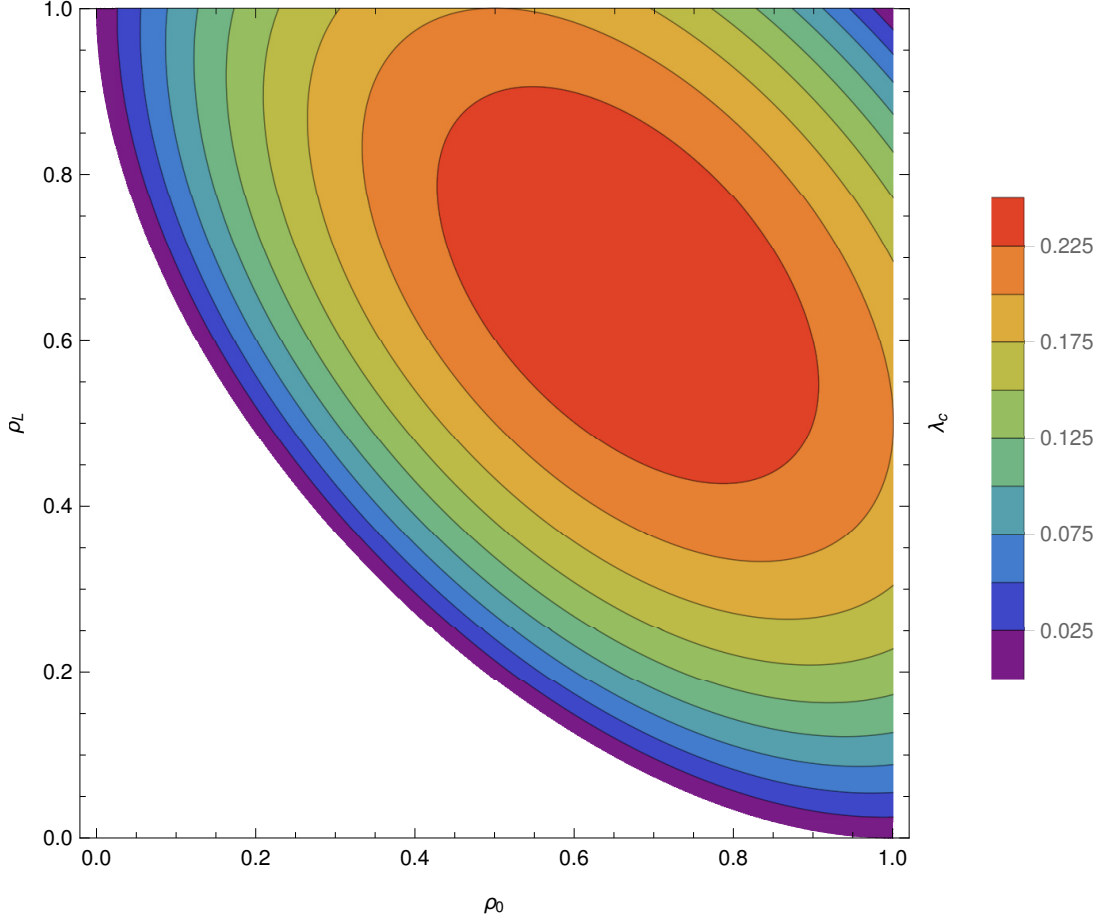
$$\bar{\rho} = \frac{6(\rho_0 + \rho_L) + \zeta [9(\rho_0^3 + \rho_L^3) - 16(\rho_0^2 + \rho_L^2) + \rho_0\rho_L(9[\rho_0 + \rho_L] - 16)]}{12[1 + \zeta(\rho_0^2 + \rho_L^2 + \rho_0\rho_L - 2[\rho_0 + \rho_L])]} \quad (2.36)$$

The variation of the average density with  $\lambda$  for selected fixed boundary conditions is plotted in Fig. 2.7. In general, this overall density deviates very little from the average of the two boundary densities.

### Other Analytic Solutions

Steady flow across a bounded domain is not the only solution for the continuum-limit MFT. We can also attempt to exploit Lie symmetries in the equations to generate solutions. Using the results in [2], we see that there should exist solutions of the form  $\rho(x, t) = \phi(\omega)$  with  $\omega = x - vt$  for some real  $v$ ; intuitively, this corresponds to a solution which simply translates through time with velocity

**Figure 2.6** A plot of the critical value  $\lambda_c$ , specified in Eq. 2.34 which  $\lambda$  must be smaller than in order to cause backward flow with boundary densities  $(\rho_0, \rho_L)$ . The region for which  $\lambda_c$  is negative is not included and marked in white, as  $\lambda > 0$  for a physically realistic system. This shows that there are boundary configurations for which flow should still occur for arbitrarily small values of  $\lambda$ .



v. After a little rearrangement, this implies that

$$v \frac{d\phi}{d\omega} = -\frac{a^2}{\tau_0} \frac{d}{d\omega} [1 - \zeta\phi(4 - 3\phi)] \quad (2.37)$$

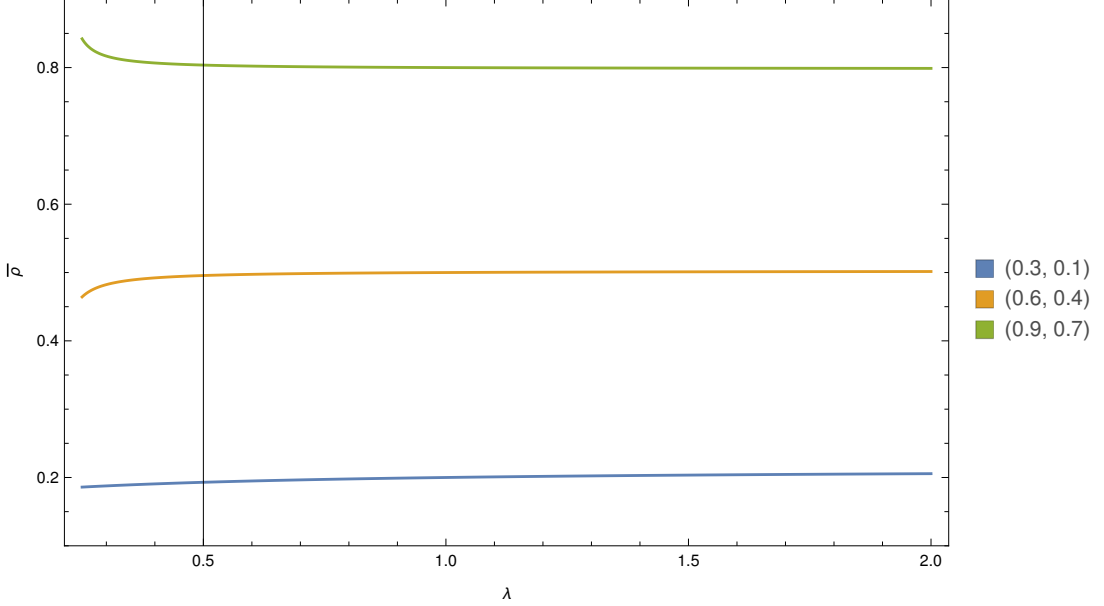
which may be integrated and then solved as a first order ODE to obtain

$$\omega = \frac{a^2}{\tau_0 v} \left[ \frac{1}{2} \zeta \phi (8 - 6\mu - 3\phi) - (1 - \zeta [4 - 3\mu] \mu) \log(\phi - \mu) \right] + \omega_0, \quad (2.38)$$

where  $\omega_0$  and  $\mu$  are constants.

Now we need as usual to consider what kind of boundary conditions to use. For simplicity, let us consider a wave of density travelling into an empty region; this implies that  $\phi \rightarrow 0$  as  $\omega \rightarrow \infty$ . The only way to achieve this is by setting  $\mu = 0$ ,

**Figure 2.7** A plot of the MFT prediction of the overall system-wide density with varying  $\lambda$  for boundaries  $(\rho_0, \rho_L) = \{(0.3, 0.1), (0.6, 0.4), (0.9, 0.7)\}$ . We have only plotted for  $\lambda > \frac{1}{4}$ , as outside this regime the MFT prediction is not unique, and so the inversion formula we need to calculate the density is not valid. In each case the density rarely deviates far from the average of the two boundary densities.



leaving us with

$$\omega(\phi) = \frac{a^2}{v\tau_0} \left[ \frac{1}{2} \zeta \phi (8 - 3\phi) - \log \phi - \frac{5}{2} \zeta \right] + \omega_0. \quad (2.39)$$

As we can vary  $\omega_0$  to shift solutions around in  $\omega$  essentially arbitrarily, we can choose where  $\phi$  takes a desired value. For convenience, let's make  $\phi$  take the value 1 at  $\omega = 0$ , which is easily achievable by setting  $\omega_0 = 0$ . At this point, we are faced with the prospect of trying to invert Eq. 2.39. This would be annoying, although one could be assisted by numerics to lighten the load. However, we can gather plenty of information simply by taking some limits. As  $\omega \rightarrow \infty$ ,  $\phi \rightarrow 0$  by design, and so  $\phi(\omega) = \mathcal{O}(e^{-\frac{v\omega\tau_0}{a^2}})$ ; having an exponential tail at the leading edge of the wave, with a thickness proportional to the default diffusion coefficient divided by the wave speed, makes perfect sense. Meanwhile, by considering small variations in  $\phi$  around 1, we may derive that  $\phi \sim 1 - \frac{v\tau_0}{a^2\lambda}\omega$  as  $\omega \rightarrow 0$ . One could see this as being a front, behind which the system is filled by a blast wave moving with velocity  $v$ . Notice how both limits suggest that the leading edge of the wave becomes thinner with increasing wavespeed, whilst close to the full region it thickens in proportion to  $\lambda$ .

However, we are left with the problem that we have the free parameter  $v$  in the solution. One might hope that we can find the preferred value for  $v$  by means of a speed-selection argument as is done with the Fisher-KPP equation [5], but that does not work in this case as the wave tail thickness is monotonic in the wave speed. Therefore, the wave speed seems to be dictated by the initial conditions, which allows some rather bizarre behaviour. For example, in the limit  $v \rightarrow +\infty$ , the initial condition (in other words, setting  $t = 0$  and observing that  $\rho(x, 0) = \phi(x)$ ) resembles an inverted Heaviside step function for  $x > 0$ ; thus this suggests that if we were to start the system with initial condition  $\rho(x, 0) = 1 - H(x)$ , the high-density region would advance into the low-density region with infinite velocity, regardless of  $a$ ,  $\tau_0$  or  $\lambda$ . This seems somewhat unphysical, and serves as a reminder that the MFT is a guide only, and shouldn't be expected to accurately predict the behaviour of the SPM.

Using [2] there is one last type of solution based upon symmetry. To acquire it, let us define  $\xi = \frac{x}{\sqrt{t}}$  and  $\rho(x, t) = \chi(\xi)$ ; then our PDE reduces to

$$\xi \frac{d\chi}{d\xi} = -2 \frac{a^2}{\tau_0} \frac{d}{d\xi} [1 - \zeta\chi(4 - 3\chi)]. \quad (2.40)$$

Taking  $\zeta = 0$ , this clearly reduces to the standard similarity solution of the diffusion equation as we would expect, so this is the nonlinear analogue of that. Unfortunately, this is a nonlinear second order ODE which isn't particularly amenable to solution, so after some solution attempts we decided to give up at this point and focus on numerics and other analytic avenues.

### 2.3.5 Implications of Continuum MFT Breakdown

We have already mentioned that the MFT can predict negative diffusion coefficients for  $\lambda < \frac{1}{4}$ ,  $\rho \in (\rho_-, \rho_+)$  as defined in Eq. 2.27. However, we should investigate this in a little more detail, as it has testable implications for the SPM.

Treating the MFT at face value, our stability analysis in 2.3.3 suggests that in the event that we have a region with  $\rho \in (\rho_-, \rho_+)$  there should be a tendency for the medium to separate into parts which have  $\rho \notin (\rho_-, \rho_+)$ ; of course, the first  $\rho$ s for which  $\rho \notin (\rho_-, \rho_+)$  are  $\rho_-$  and  $\rho_+$  themselves, which are the values for which the diffusion coefficient, and therefore the current resulting from a concentration gradient is zero. So, the process of the medium separating should in general yield

a mixture of regions with  $\rho = \rho_-$ ,  $\rho = \rho_+$  and other  $\rho \notin (\rho_-, \rho_+)$ , mixed in such a way that the total number of particles is locally conserved.

It is this nonuniqueness of configuration which causes us some problems if we try to accept the MFT as a good descriptor of SPM phenomenology. In reference to our steady state solution described in 2.3.4, note that  $\rho(x)$  is only unique so long as we avoid negative diffusion, otherwise, the cubic inversion we need to perform to transform  $x(\rho)$  into  $\rho(x)$  is multivalued. One could imagine that we could fix this by patching together sections which cross with  $\rho = \rho_-$  or  $\rho_+$ , but then we have essentially unlimited choice of how large to make the sections and how many alternations to include. This means that the MFT makes no prediction of the system-wide average density  $\bar{\rho}$  which is unfortunate as this is a quantity which it is easy for us to measure using our numerics.

## 2.4 The SPM in Higher Dimensions

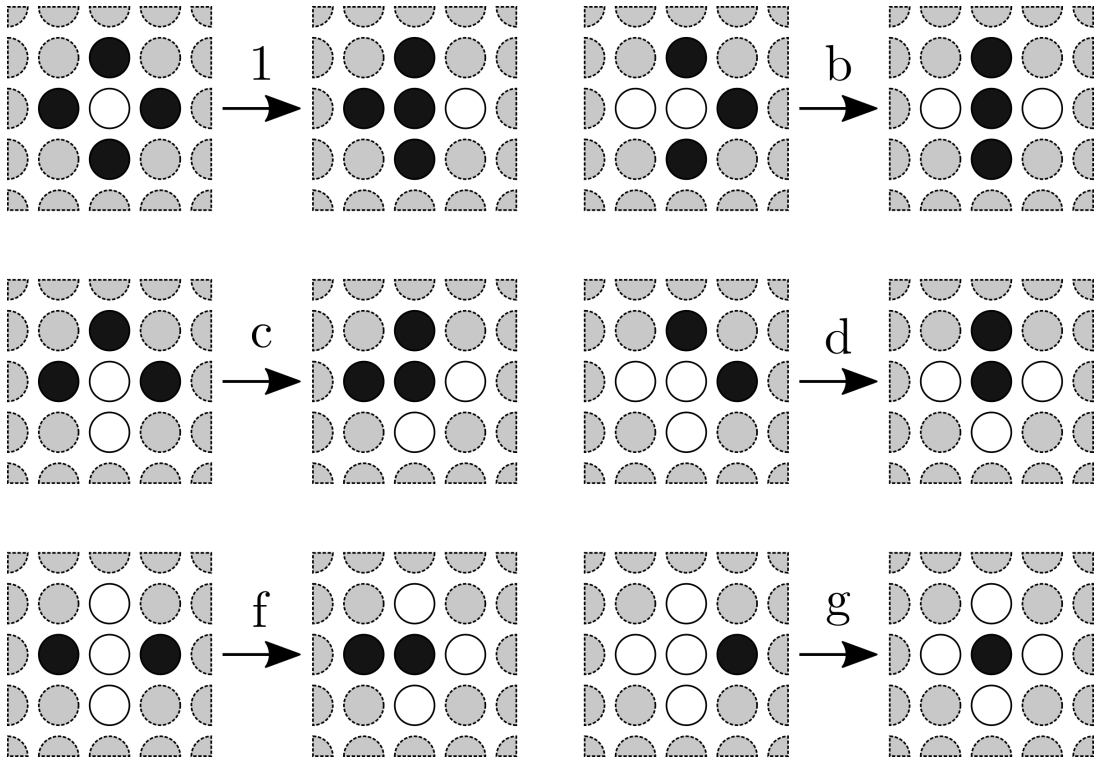
We initially designed the SPM for use in one dimension, as it was originally intended to represent interacting particles moving along a periodic potential with deep, narrow wells. However, it is only natural to wonder whether a similar model could be constructed in higher dimensions. Recall that the SPM in one dimension was designed to have two properties:

- Left-right symmetry, and
- locality, in the sense that only the presence or absence of a particle in an adjacent lattice site may influence the transition rate.

In addition we also proved that (boundary conditions aside) the SPM also obeys detailed balance. This was not put into the model intentionally, but emerges naturally as the space of possible one-dimensional models which are local and symmetric is very small. Let us consider only square lattices in  $n$  dimensions, for simplicity. If we attempt to build a model in two dimensions which is symmetric and local, (i.e. obeys all the point group symmetries of the underlying lattice, and whose transitions are only influenced by the immediate environment around a particle), we find that we now have more freedom in the model construction than we did in one dimension. For example, in two dimensions a moving particle might be leaving any one of six possible unique local configurations, as shown in Fig. 2.8,

and so such a model would need to be parametrised by 5 rates, once we take time dilation symmetry into account. The number of possible symmetric local hopping models only grows greater in higher dimensions, and this makes it very difficult to analyse the parameter space of such models using numerics. Therefore, we have chosen to investigate most closely those models which in addition obey detailed balance; as it turns out, there is only one such model, regardless of the number of dimensions.

**Figure 2.8** *The unique available moves in a 2-dimensional symmetric local hopping model. Note that we have rescaled time so that the free particle hopping rate is 1, for consistency with the 1-dimensional SPM. Simultaneous rotations or reflections of both initial and final states are also allowed moves with the same rates. White corresponds to a lattice site occupied by a particle, black to an unoccupied site, and grey to a site which has no effect on the transition rate. In each case a particle moves into an empty space to its right, with its different starting environment determining the transition rate.*



### 2.4.1 Symmetry + Locality + Detailed Balance = Unique 1-Parameter SPM

When investigating higher-dimensional analogues of the SPM, we initially considered a generic model as shown in Fig. 2.8; however, as the parameter space is so large, we decided to attempt to impose the detailed balance condition and see how much freedom that gave the model. In the end, after some exceedingly tedious casework, we found that in order to obey detailed balance particles needed to move with transition rate specified by the following theorem, which applies in arbitrary numbers of dimensions:

**Theorem 1.** *Any processes defined on an  $n$ -dimensional square lattice in which particles swap places with vacancies and whose transition rates  $\sigma(\xi_1 \rightarrow \xi_2)$*

- *are symmetric (invariant under rotations, reflections and translations of the underlying lattice),*
- *local (rate at which a particle swaps with a vacancy only depends upon configuration of particle's immediate neighbours),*
- *and obey detailed balance, i.e. that  $\exists$  probability distribution  $P$  over configurations  $\xi \in \Xi$  such that  $\forall \xi_1, \xi_2 \in \Xi$ ,*

$$P(\xi_1)\sigma(\xi_1 \rightarrow \xi_2) = P(\xi_2)\sigma(\xi_2 \rightarrow \xi_1) \quad (2.41)$$

*must have a transition rate of the form*

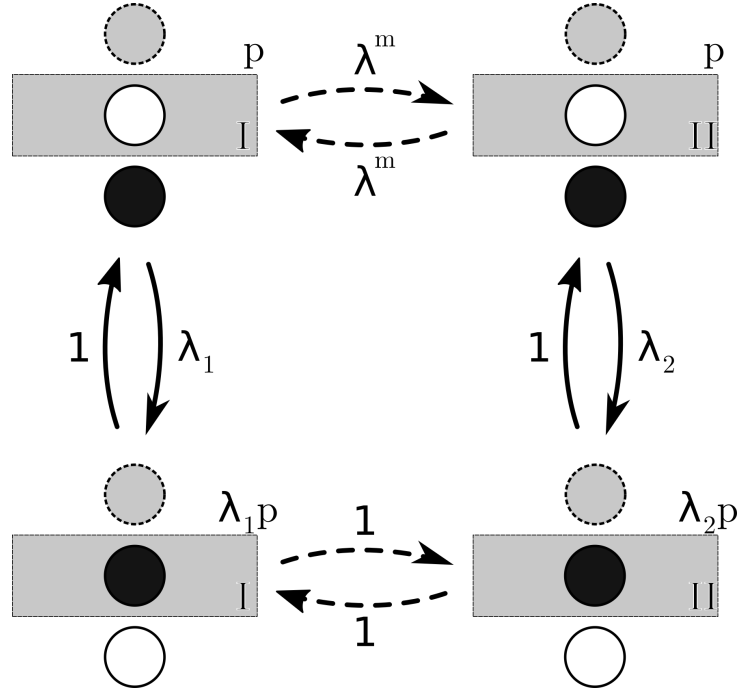
$$\sigma(\xi_1 \rightarrow \xi_2) = \frac{1}{\tau_0} \lambda^m, \quad (2.42)$$

*where  $m$  is the number of particles directly adjacent to the particle which is attempting to swap with a vacancy and  $\tau_0$  is an arbitrary constant.*

*Proof.* We have already shown that the theorem applies in 1-dimension, as there the space of possible models is so constrained [reference in introduction] that there is only one symmetric local model, which is the SPM. This model, as we showed, obeys detailed balance anyway, so we're done for  $n = 1$ .

We will proceed with the proof via induction. Let us assume that the result is true in  $(n - 1)$  dimensions. Firstly, we need to show that the actual configuration

**Figure 2.9** *I and II represent two local configurations of  $m$  particles, centred around a single site, which may or may not be occupied, in an  $(n-1)$ -dimensional hyperplane intersecting the central site. The dotted lines dashed arrows represent configurational transitions which require multiple steps, all with the same rate (in this case,  $\lambda$ ) as indicated. The grey particle slot represents a slot whose occupation is irrelevant for this calculation, although it must be constant throughout. The expressions in the top right corners of the configurations are the probabilities of our finding the system in that configuration.*



of the particles in contact with a particle does not affect its rate of motion into an adjacent free space. Fig. 2.9 shows just such a situation: there are  $m$  particles clustered around the central particle in an  $(n-1)$ -dimensional hyperplane, but in two different local configurations, I and II. Because the model in  $(n-1)$ -d obeys detailed balance, we can consider a reversible chain of moves from one configuration to the other. We do this by moving each particle adjacent to the central particle outwards, with rate  $\lambda$ . Once they are all separated from the central particle, we can then move them around at leisure, with each move having rate 1 so long as we keep them separate; luckily, there is plenty of room to do this, as we can simply move the particles further away using only rate 1 moves. We can then rebuild the particles from, say, configuration I into their exact state in configuration II. Furthermore, we can do exactly the same thing going from configuration II to configuration I, again using only  $m$  rate  $\lambda$  moves and the rest with rate 1. Importantly, if a system obeys detailed balance, then if we can move

from one state to another and back again with the same rate, they must have the same equilibrium occupation; therefore, the probability of finding the system in configuration I and the probability of finding it in configuration II must be equal, otherwise the system would violate detailed balance (which the model which we are assuming the system obeys in  $(n - 1)$ -d satisfies). However, there is another way to go from state I to state II: we can move the central particle, which we will say occurs with rates  $\lambda_1$  and  $\lambda_2$  respectively. Once the central particle is moved, we now have a “gas” of free particles, which we can once again move as we like using only moves of rate 1, in order to deform the system into configuration II. As the probability of our system being in state II is the same as it being in state I, the only way detailed balance can be obeyed is if  $\lambda_1 = \lambda_2$ . Therefore, the rate at which a particle moves into an adjacent empty space cannot depend upon the configuration of its adjacent particles in a given  $(n - 1)$ -dimensional hyperplane, only their number.

Now we need to consider two cases, as the slot directly behind the central particle’s proposed direction of motion can be either empty or full. Firstly, the empty case is considered in Fig. 2.10. This time, we are highlighting the fact that if we move the central particle out of a hyperplane configuration of  $m$  particles, which occurs with rate  $u_m$ , this results in a gas of free particles; equivalently we could’ve produced a gas by moving the adjacent particles one by one as before, which requires  $m$  steps with each with rate  $\lambda$ . As the two gases are equivalent, in detailed balance terms, they must have the same realisation probability. If the probability of our being in the initial configuration (top left) was  $p$ , then by detailed balance the probability of our being in a free particle state is simultaneously both  $pu_m$  and  $p\lambda^m$ , and so  $pu_m = p\lambda^m$  implying that

$$\lambda^m = u_m. \quad (2.43)$$

In Fig. 2.11, we show exactly the same thing, only this time there is a particle behind the central particle, and so an additional move must be made in order to create a gas of free particles. This means that the equivalence is now between  $pu_m$  and  $p\lambda^{m+1}$ , and so

$$\lambda^{m+1} = w_m. \quad (2.44)$$

With the constraints that detailed balance imposes upon  $u_m$  and  $w_m$ , we find that the original proposition for dimension  $n$  is true so long as it is for dimension  $(n - 1)$  for  $n > 1$ , and as we know it is true for  $n = 1$ , the theorem is proved.

**Figure 2.10** Here we've used the same diagram rules as in Fig. 2.9.

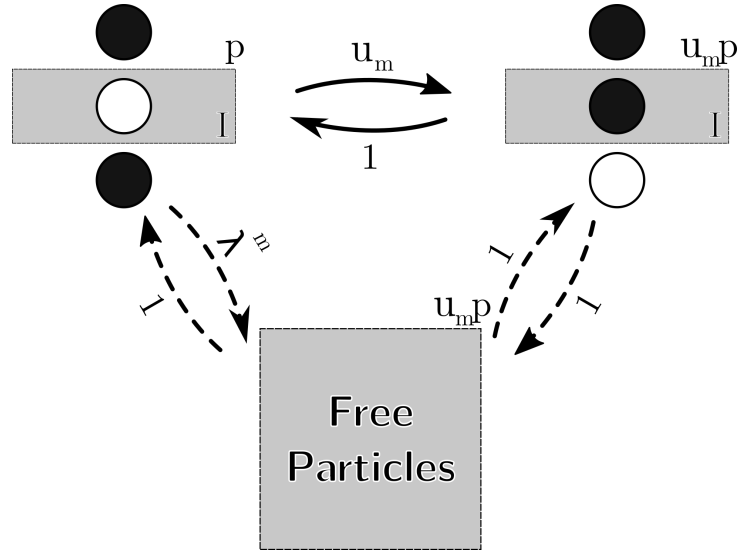
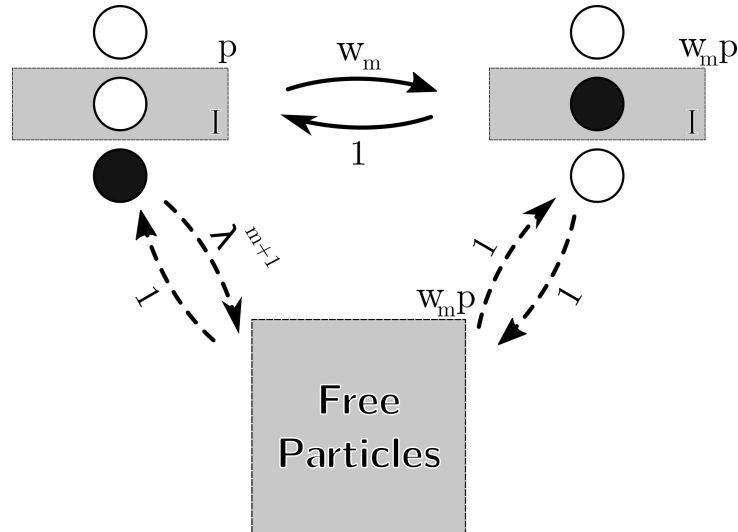


**Figure 2.11** As Fig. 2.10, but now with a particle behind the central one.



□

Theorem 1 implies that an  $n$ -dimensional exclusion model which is symmetric, local and obeys detailed balance must have an energy (defining the equilibrium distribution) which is proportional to the number of particle-particle adjacencies in the system; this therefore limits energy to being contained in the “bond” between adjacent particles, leaving us only with the option of a simple additive bond energy. This means that in order to have a more complicated energy, our only option is to either break symmetry or have a system of rates which considers

more than the immediate environment of a particle which is attempting to move, for example considering the environment to which the particle is going.

The advantage of possessing this result is that it highlights that in  $n$ -dimensions there is again a special, simple one-parameter model which has many symmetry properties and is therefore a good first target for study. As such, we will perform a mean-field analysis of the  $n$ -dimensional SPM, to give us analytical results to compare to later Monte-Carlo numerics.

### 2.4.2 MFT of the $n$ -Dimensional SPM

In the same manner as in Sec. 2.3.1, we will let  $\rho_\chi(t)$  be the mean occupation of the  $\chi^{\text{th}}$  site at time  $t$ , where  $\chi \in \mathbb{Z}^n$ . Let the unit vector in the  $i^{\text{th}}$  direction be  $e_i \in \mathbb{Z}^n$ , so that  $\rho_{\chi+e_i}$  refers to a lattice site adjacent to the  $\chi^{\text{th}}$  and offset in the  $i^{\text{th}}$  direction. Then, making the normal MFT assumption (that means of products are products of means), we can say that the rate at which a particle moves from site  $\chi$  to site  $\chi + e_i$  is

$$\begin{aligned} \sigma_{\chi \rightarrow \chi + e_i} &= \rho_\chi(1 - \rho_{\chi + e_i}) [(1 - \rho_{\chi - e_i}) + \lambda \rho_{\chi - e_i}] \\ &\times \prod_{j \neq i}^n [(1 - \rho_{\chi + e_j})(1 - \rho_{\chi - e_j}) + \lambda \rho_{\chi + e_j}(1 - \rho_{\chi - e_j}) + \lambda \rho_{\chi - e_j}(1 - \rho_{\chi + e_j}) + \lambda^2 \rho_{\chi + e_j} \rho_{\chi - e_j}] \\ &= \rho_\chi (1 - \rho_{\chi + e_i}) [1 - \zeta \rho_{\chi - e_i}] \prod_{j \neq i}^n [(1 - \zeta \rho_{\chi - e_j})(1 - \zeta \rho_{\chi + e_j})], \end{aligned} \quad (2.45)$$

with  $\zeta = 1 - \lambda$  as usual.

Again, we will move to a continuum formulation. To do this, we are best off considering the overall flow between the site at  $\chi$  and the site at  $\chi + e_i$ , and then Taylor expanding  $\rho(\mathbf{x}, t)$  as a continuous variable. Doing this analytically in arbitrary dimensions is extremely tedious, and more importantly error-prone; thus, computer assistance is useful. A code which calculates this MFT current for given  $n$  to  $\mathcal{O}(a^3)$  may be found in Sec. A.2.

Computing this current for a few low values of  $n$ , a pattern emerges, as one can see in Tab. 2.1. Thus one can see that the MFT current in  $n$ -dimensions is

$$\mathbf{J} = -\frac{a^2}{\tau_0} (1 - \zeta \rho)^{2(n-1)} [1 - \zeta \rho ((2n+2) - (2n+1)\rho)] \nabla \rho, \quad (2.46)$$

**Table 2.1** The MFT current in the SPM, as a function of the density gradient, for the first 4 dimensions.

n	Simplified Current, $-\mathbf{J} \frac{\tau_0}{a^2}$
1	$[1 - \zeta\rho(4 - 3\rho)] \nabla\rho$
2	$(1 - \zeta\rho)^2 [1 - \zeta\rho(6 - 5\rho)] \nabla\rho$
3	$(1 - \zeta\rho)^4 [1 - \zeta\rho(8 - 7\rho)] \nabla\rho$
4	$(1 - \zeta\rho)^6 [1 - \zeta\rho(10 - 9\rho)] \nabla\rho$

where the current and density obey the usual continuity equation

$$D = \frac{\partial\rho}{\partial t} + \nabla \cdot \mathbf{J} = 0 \quad (2.47)$$

with  $\mathbf{J} = -D(\rho)\nabla\rho$ ,  $D$  being the diffusion coefficient

$$\frac{a^2}{\tau_0} (1 - \zeta\rho)^{2(n-1)} [1 - \zeta\rho((2n+2) - (2n+1)\rho)]. \quad (2.48)$$

The equivalent of our 1-dimensional steady state solution may be found by considering a flow from one hyperplane to a parallel one a distance  $L$  away. Taking the planes to be separated in the  $x$  direction, we find that we have an equivalent solution, where the homogeneous current  $J_0$  is given by

$$J_0 = \int_{\rho_L}^{\rho_0} d\rho \frac{a^2}{L\tau_0} (1 - \zeta\rho)^{2(n-1)} [1 - \zeta\rho((2n+2) - (2n+1)\rho)] \quad (2.49)$$

and the density profile is the implicit solution of

$$\int_{\rho}^{\rho_0} d\rho \frac{a^2}{\tau_0} (1 - \zeta\rho)^{2(n-1)} [1 - \zeta\rho((2n+2) - (2n+1)\rho)] = J_0 x. \quad (2.50)$$

### **Limiting and Symmetry Properties of the $n$ -Dimensional MFT**

Now that we have derived the diffusion coefficient  $D$  in the  $n$ -dimensional MFT, we can investigate some special cases, in a similar manner to the 1d situation.

As  $\rho \rightarrow 0$ ,  $D \rightarrow 1$ , which makes sense as in extremely low-density situations the particles do not interact. As  $\rho \rightarrow \frac{a^2}{\tau_0}$ ,  $D \rightarrow \lambda^{2(n-1)} \frac{a^2}{\tau_0}$ , which again corresponds to the diffusion of vacancies in an almost-full lattice (which depends upon almost

fully-bound particles needing to jump in order for a vacancy to move).

However, unlike the 1d situation, there is no longer a symmetry in the density dependence of the diffusion coefficient. This is because the  $(1 - \zeta\rho)^{2(n-1)}$  bracket is symmetric about  $\rho = \zeta^{-1}$ , whereas the  $[1 - \zeta\rho((2n+2) - (2n+1)\rho)]$  bracket's symmetry is about  $\rho = \frac{n+1}{2n+1}$ ; thus, in general they would not share a point of symmetry, and so their product would not be symmetric.

Finding the density at which flow is extremal is annoying, but doable. Differentiating the diffusion coefficient with respect to  $\rho$  gives, after factorising,

$$\frac{\partial D}{\partial \rho} = -2\zeta(1 - \zeta\rho)^{2n-3} [\zeta\rho(n(2n+1)(\rho-1)+1) - 2n(\rho-1) - \rho]. \quad (2.51)$$

The first bracket has its zero when  $\rho = \zeta^{-1}$ , which means that this only causes a turning point for allowed  $\rho$  when  $\zeta > 1$ . The second bracket is a quadratic in  $\rho$ . Its solution for  $\lambda > 0$  is

$$\frac{4}{2\zeta n^2 + (3 - \lambda)n + \lambda + \sqrt{(2\zeta n^2 + (3 - \lambda)n + \lambda)^2 - 8\zeta n(2n + 1)}} \quad (2.52)$$

### The SPM MFT in 2-Dimensions

Specifically, in the 2-dimensional case,  $J_0$  is given by

$$J_0 = \frac{a^2}{L\tau_0} \left[ \zeta^3 (\rho_0^5 - \rho_L^5) + \frac{1}{2}\zeta^2 (3\zeta + 5) (\rho_L^4 - \rho_0^4) + \frac{1}{3}\zeta (13\zeta + 5) (\rho_0^3 - \rho_L^3) + 4\zeta (\rho_L^2 - \rho_0^2) + (\rho_0 - \rho_L) \right]. \quad (2.53)$$

The dependence of flow upon the boundary conditions for some given  $\lambda$  is shown in Figure. 2.12, and the dependence of flow upon  $\lambda$  for some fixed boundaries is shown in Fig. 2.13. We can use these in comparison with our Monte-Carlo data in 2-dimensions.

**Figure 2.12** Plots of the flow in the MFT of the 2-dimensional SPM, where we are varying the boundary densities. The values of  $\lambda$  used are  $\{0.2, 0.4, 0.75, 2\}$ , going clockwise from top left.

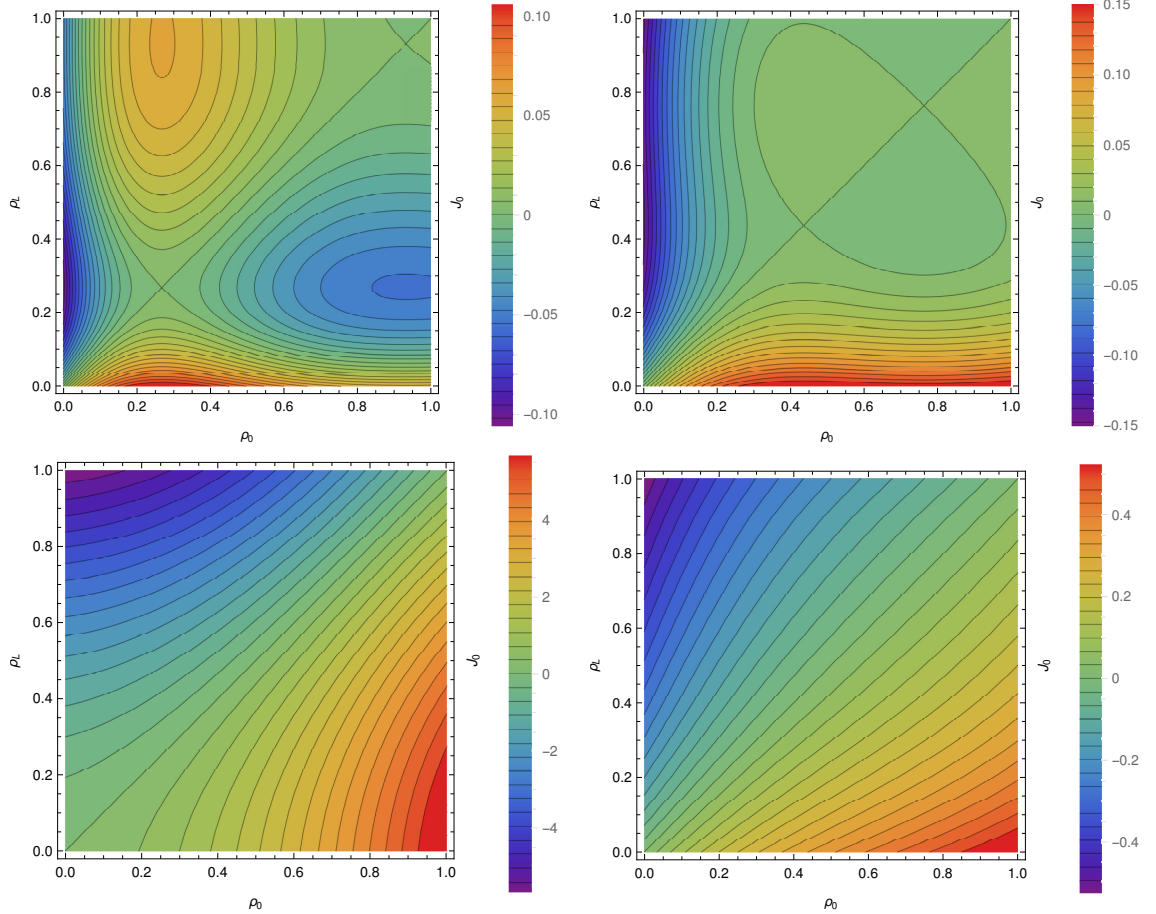
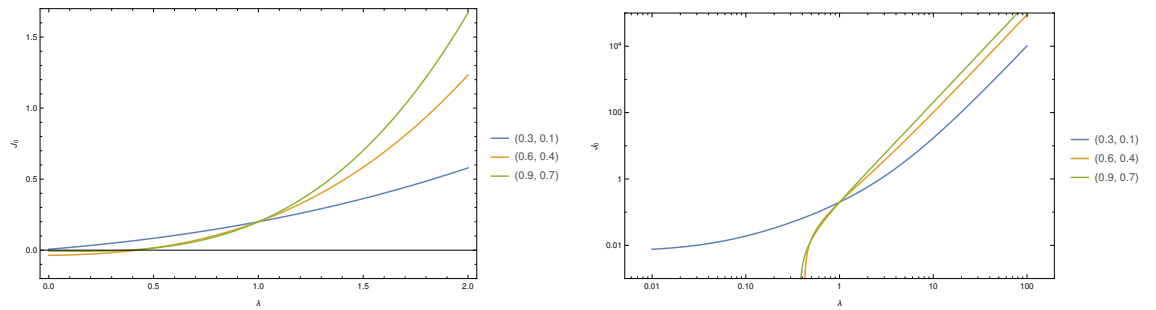


**Figure 2.13** Plots of the current variation with respect to  $\lambda$  in the MFT of the 2-dimensional SPM. Boundary conditions are labelled in the legend in the form  $(\rho_0, \rho_L)$ .



# **Chapter 3**

## **Numerical Results about the SPM**

### **3.1 Numerical Simulations of Continuous-Time Markov Processes**

#### **3.1.1 Known Methods**

Discuss commonly-used methods, and how they work. Eventually, talk about why we are using the n-fold way.

#### **3.1.2 KMCLib**

Talk about how it works, why I picked it over other implementations.

#### **3.1.3 Running KMCLib on Eddie3**

How calculations are managed day-to-day.

## **3.2 Calculation Results**

### **3.2.1 1D**

### **3.2.2 2D**

# **Chapter 4**

## **Conclusions**

Need to summarise the key results of the research here, and give an overview.

# Appendix A

## Code Listings

### A.1 1d Ising Correlation Functions

This Python script computes the probability of a site being occupied  $l$  lattice spacings away from an occupied site. It requires the system size  $L$  and the number of particles  $N$  as inputs. The output is saved in a file called `corrFnResults.m`, which is formatted so that it may be used by **Mathematica**.

```
import copy
import sys

def configMake(L, N, prevList, totList):
    if L==1:
        endList = [copy.deepcopy(prevList), N]
        totList.append(unfold(endList))
        return [N]
    if N==0:
        return configMake(L-1, 0, [copy.deepcopy(prevList), 0], totList)
    if L==N:
        return configMake(L-1, N-1, [copy.deepcopy(prevList), 1], totList)
    return [configMake(L-1, N, [copy.deepcopy(prevList), 0], totList),
            configMake(L-1, N-1, [copy.deepcopy(prevList), 1], totList)]

def adjSum(candList):
    listLen = len(candList)
    total = 0
    for index in range(0, listLen):
        total += candList[index-1]*candList[index]
    return total

def unfold(candList):
    if isinstance(candList, list):
        if len(candList)==2:
            return unfold(candList[0])+unfold(candList[1])
```

```

        if len(candList)==1:
            return candList
        if len(candList)==0:
            return []
        return [candList]

def listCollate(candList):
    maxItem = 0
    for index in candList:
        if index > maxItem:
            maxItem = index
    outPut = []
    for size in range(0, maxItem+1):
        numCounts = 0
        for index in candList:
            if index == size:
                numCounts += 1
        outPut.append((size, numCounts))
    return outPut

def genCorrFn(L, N):
    totList = []
    allStates = configMake(L, N, [], totList)
    restStates = []
    weightList = []
    maxAdj = 0
    for state in totList:
        if state[0]==1:
            restStates.append((state, adjSum(state)))
            if restStates[-1][1]>maxAdj:
                maxAdj = restStates[-1][1]
            weightList.append(restStates[-1][1])
    partFnList = listCollate(weightList)
    print(partFnList)
    partitionFn = "("
    for pair in partFnList:
        partitionFn += str(pair[1])+" \u2202Exp ["+str(pair[0]-maxAdj)+ "b] \u2202 + "
    partitionFn += "0)"
    print(partitionFn)
    finalOut = "{"
    for shift in range(0, L-L/2):
        tempList = []
        for config in restStates:
            if config[0][shift] == 1:
                tempList.append(config[1])
        stateDist = listCollate(tempList)
        outSum = "{"+str(shift)+", "
        for pair in stateDist:
            outSum += str(pair[1])+" \u2202Exp ["+str(pair[0]-maxAdj)+ "b] \u2202 + "
        outSum += "0) / "+partitionFn+"}"
        finalOut += outSum
        if shift != L-L/2-1:
            finalOut += ", "
    finalOut+="}"
    return finalOut

L = int(sys.argv[1])

```

```

with open("corrFnResults.m", 'w') as f:
    f.write("{")
    for n in range(2, L-2):
        f.write("{"+str(n)+"/"+str(L)+" , "+genCorrFn(L, n)+"}, ")
    f.write(genCorrFn(L, L-2) + "}")

```

## A.2 $n$ -Dimensional Continuum-Limit MFT

This Mathematica script computes the current which flows between two adjacent sites (offset in the  $e_1$  direction) in the MFT of the  $n$ -dimensional SPM; due to symmetry, this tells us what happens in an arbitrary direction. In this case  $n$  is set to 3, but it still works if changed to any positive number.

```

n = 3;
i = 1;
zero = 0*UnitVector[n, 1];
e[i_] := UnitVector[n, i];
Hess = Table[
  Piecewise[{{d2p[j, i], j > i}}, d2p[i, j]], {i, 1, n}, {j, 1, n}];
Jacob = Table[dp[i], {i, 1, n}];
p[x_] := p0 + Jacob.x + 1/2 x.(Hess.x);
rightJ = 1/
  t0 (1 - p[1/2 a e[i]]) p[-(1/2) a e[i]] (1 -
  z p[-(3/2) a e[i]]) Product[
  Piecewise[{{(1 - z p[-a e[j] - 1/2 a e[i]]) (1 -
  z p[a e[j] - 1/2 a e[i]])}, {j != i}}, 1], {j, 1, n}];
leftJ = 1/t0 (1 - p[-(1/2) a e[i]]) p[
  1/2 a e[i]] (1 - z p[3/2 a e[i]]) Product[
  Piecewise[{{(1 - z p[-a e[j] + 1/2 a e[i]]) (1 -
  z p[a e[j] + 1/2 a e[i]])}, {j != i}}, 1], {j, 1, n}];
fullJ = rightJ - leftJ + 0[a]^3;
FullSimplify[fullJ]

```

# Bibliography

- [1] Evans, M. R., and B. Waclaw. “Condensation in stochastic mass transport models: beyond the zero-range process.” *Journal of Physics A: Mathematical and Theoretical* 47, 9: (2014) 095,001. <http://stacks.iop.org/1751-8121/47/i=9/a=095001>.
- [2] Ivanova, N. M. “Exact solutions of diffusion-convection equations.” *arXiv preprint arXiv:0710.4000* <https://arxiv.org/abs/0710.4000>.
- [3] Laisant, C.-A. “Intgration des fonctions inverses.” *Nouvelles annales de mathmatiques : journal des candidats aux coles polytechnique et normale* 5: (1905) 253–257. <http://eudml.org/doc/101975>.
- [4] Landau, L. D., E. M. Lifshitz, and L. Pitaevskii. “Statistical physics, part I.”, 1980.
- [5] Sherratt, J. A. “On the transition from initial data to travelling waves in the Fisher-KPP equation.” *Dynamics and Stability of Systems* 13, 2: (1998) 167–174. <https://doi.org/10.1080/02681119808806258>.